



Geometrically nonlinear deflection and stress analysis of skew sandwich shell panel using higher-order theory

Pankaj V. Katariya¹ · Chetan K. Hirwani¹ · Subrata K. Panda¹

Received: 24 January 2018 / Accepted: 11 April 2018 / Published online: 19 April 2018
© Springer-Verlag London Ltd., part of Springer Nature 2018

Abstract

The nonlinear static responses of the skew sandwich flat/curved shell panel including the corresponding stress values are examined in this article under the influence of the unvarying transverse mechanical load. To evaluate the said responses of the sandwich panel, the physical structure model turned to a mathematical form via a higher-order kinematic theory including the stretching term effect in the displacement field variable. The effect of geometrical nonlinearity has been included via Green–Lagrange strain–displacement kinematics. The governing equation has been derived from the variational principle and is solved via direct iterative technique including the finite element procedure. Further, a customized finite element computer code has been developed in MATLAB environment based on the current mathematical model for the computational purpose. To check the comprehensive behavior of the proposed model, the bending responses are obtained for different mesh sizes and compared with the published data (numerical and 3D elasticity solution). Subsequently, a wide range of numerical examples have been solved for the different geometrical configurations (side-to-thickness ratio, curvature ratio, core-to-face thickness ratio, skew angle and support conditions) and the influence of the same on deflection and stress behavior has been shown and discussed in detail.

Keywords Bending · Equivalent single layer · Skew · Green–Lagrange · HSDT

1 Introduction

In the recent years, the use of laminated and sandwich composite structures in high-performance engineering fields such as aerospace, automotive and naval industries has been increased greatly due to their superior performance and reliability. In general, the low specific weight with higher specific strength is the prime requirement of the discussed industries and due to which the sandwich composites are preferable. In addition, the geometry (the length and the width) of the structural element used in such weight sensitive industries are not necessarily perpendicular to the each other. They might be in some angle or in other word skewed. The examples of such panel are swept wings, skin panels of aircraft, etc. These panels are usually thin and their deflections are quite large in comparison to their thickness. Similarly, when they are exposed to the service condition experiences different

kinds of loading. Hence, to analyse the structural behaviour (large deformation), a nonlinear analysis must be used. In this regard, i.e., to improve the comprehensive knowledge on the structural behavior including the effect of large deformation and to predict the same accurately, many mid-plane kinematic theories (higher-order shear deformation theory, HSDT; first-order shear deformation theory, FSDT; zig-zag theory, layerwise theory, LW and refined higher-order or zig-zag theories) have been developed every now and then. Now, a review of the important contribution using above discussed theories is present in the following line to find out the knowledge gap and to establish the objective and necessity of the present work.

The composite and sandwich structures have been modeled extensively to examine the associated responses (bending, vibration and buckling) by every now and then using the established as well as modified kinematic theories for the accurate evaluation. In this regard, few relevant articles are discussed in the following lines to establish the knowledge gap. The large deformation bending responses including the coupled environmental effect on the laminated composites and sandwich structure are analysed analytically [1, 2] using

✉ Subrata K. Panda
pandask@nitrkl.ac.in

¹ Department of Mechanical Engineering, National Institute of Technology Rourkela, Rourkela, Odisha 769008, India

the perturbation technique as well as derived new axiomatic plate theory [3] for the modeling purpose. The prediction of the deflection and the frequency responses the cross-ply laminated and sandwich plates presented using a layer-wise theory with a generalized differential quadrature (GDQ) technique [4] and the Carrera's Unified Formulation (CUF) with a radial basis function (RBF) in association with the collocation technique [5]. Similarly, the frequency responses and heat transfer rate within a three-dimensional (3-D) solid and composite structures are verified by [6] adopting the consecutive-interpolation procedure (CIP). Additionally, the study related to the strength optimization of the layered structure are reported [7] using the modified feasible direction method (MFD). Further, to improve the understanding of the laminated and sandwich composite structure with the corrugated soft core and to enhance the accuracy of computational modeling skill, the finite element method (FEM) including the commercial finite element (FE) package ANSYS [8, 9] is adopted in the past. In addition, the hybrid-stress based FEM [10] technique is adopted for the analysis of the modal response and static deflection values of the layered structure. Further, the FEM has been adopted for the computational analysis purpose of the deflection behaviour of different kind of structural geometries and construction (rectangular, stiffened annular sector plate, parallelogram-shaped plate, and sandwich plate) including the large deformation behaviour via von-Karman strain using the FSDT kinematics by [11–16]. Similarly, the FSDT kinematic model is implemented further to evaluate the deflection and frequency values of the layered composite structures [17–19] with the help of the discrete shear gap technique. As discussed earlier, the LW theory (displacement based model) in association with the FEM technique is adopted to examine the bending, vibration and buckling responses [20–22] of the laminated and sandwich composite plate structure. Further, the bending and buckling responses of the nano-sandwich plate structure is examined [23] based on various kind of mid-plane kinematic models (refined zigzag theory; RZT, sinusoidal shear deformation theory; SSDT, classical plate theory; CPT and the FSDT) including solution techniques (differential cubature; DC, differential quadrature; DQ and harmonic differential quadrature; HDQ) to demonstrate the accuracy and computational effort. Further, the mechanical structural responses are computed numerically via the FEM for the laminated, sandwich and the functionally graded material (FGM) structure [32] using the kinematic models i.e. generalized layer-wise HSDT, the higher-order zigzag theory (HOZT) and inverse hyperbolic shear deformation theory (IHSDT). The linear/nonlinear structural behaviour of the functionally graded plate/sandwich beam structure are also examined using the third-order shear deformation plate theory (TSDPT) [33, 34], an efficient mesh-free method [35, 36] and isogeometric analysis approach [37, 38]. The effect of ply angle on the minimum buckling load of

the symmetrically stacked layered structure has been studied using the robust design optimization (RDO) [39] technique. In addition, the HSDT kinematic model has been adopted to study the nonlinear static and dynamic responses of the laminated composite curved shell panel [40] and skew sandwich plates [41] including the geometrical nonlinearity of the structure via von-Karman strain. In continuation to that the structural responses (static, frequency and buckling) of the laminated composite and sandwich plate have also been examined using the HSDT kinematic based IGA [42, 43], mesh-free [44, 45] and polygonal [46] approach. Similarly, few research are reported on the nonlinear transverse bending behaviour of the laminated composite shell structures [47–49] using the HSDT kinematics and Green–Lagrange nonlinear strain equation.

The current review clearly indicates two major lacunae regarding the analysis of the bending behaviour of the skew and non-skew layered structures. First, regarding the mid-plane kinematics, i.e., the static deflection is studied extensively using the FSDT kind of mid-plane theories whereas the study using the HSDT is limited. Second, the large deformation is considered via von-Karman type of strain–displacement equations for layered and sandwich plate structure only in few studies. Therefore, it is easy to point out the gap between the reported research that none of the articles discussed the non-linear static analysis of the skew sandwich shell panel using the higher-order mid-plane kinematics and Green–Lagrange strain–displacement relation. Hence, the aim of the current study is to derive a new generalized model of the skew sandwich shell structure using Green–Lagrange strain kinematics in the framework of the higher-order mid-plane theory. The current model included all of the nonlinear higher-order strain terms to achieve the necessary generality for the accurate modeling. The nonlinear responses are obtained computationally using a suitable computer code for the structural equilibrium equations with the help of isoparametric FEM steps and the direct iterative method. Moreover, the current numerical model incorporated the thickness stretching term effect for precise prediction of the deflection parameter. Further, the responses are evaluated using the newly developed nonlinear sandwich panel model and verified with those of the available published results. After showing the required accuracy of the currently developed numerical model, it is extended to compute the deflection characteristics of the skew sandwich structure for the important geometrical parameters including the skew angle and core thickness.

2 Theory

The geometrical configuration of the sandwich composite shell panel structure is provided in Fig. 1. The length, the breadth and the thickness are denoted by the symbol ' a ', ' b '

and ‘ h ’, respectively. The total thickness of the panel is the combination of the core thickness ‘ h_c ’ and the face sheet thickness ‘ h_f ’. Further, the principal radii of the curvatures of the shell panel are defined as R_{ξ_x} and R_{ξ_y} , along the length and the width, respectively. Different geometry of the shell panel say cylindrical (Cyl), spherical (Sph), elliptical (Elpt), hyperboloid (Hyp) and flat panels flat (FP) can be achieved by altering the principal radii of curvature (Cyl, $R_{\xi_x} = R, R_{\xi_y} = \infty$; Sph, $R_{\xi_x} = R_{\xi_y} = R$; Elpt, $R_{\xi_x} = 2R, R_{\xi_y} = R$; Hyp, $R_{\xi_x} = R, R_{\xi_y} = -R$ and FP, $R_{\xi_x} = R_{\xi_y} = \infty$). Now, the necessary skew effect has been added in the current model by varying the skew (ϕ) angle and the details provided in Fig. 2.

2.1 Constitutive relation

The required constitutive relation for any arbitrary k th layer of the laminated sandwich composite face sheets is expressed [50] mathematically in the following equation by considering an arbitrary angle ‘ θ ’ of the fibre orientation as:

$$\begin{Bmatrix} \sigma_{\xi_1 \xi_1}^k \\ \sigma_{\xi_2 \xi_2}^k \\ \sigma_{\zeta \zeta}^k \\ \sigma_{\xi_2 \zeta}^k \\ \sigma_{\xi_1 \zeta}^k \\ \sigma_{\xi_1 \xi_2}^k \end{Bmatrix} = \begin{bmatrix} \bar{Q}_{11} & \bar{Q}_{12} & \bar{Q}_{13} & 0 & 0 & 0 \\ \bar{Q}_{12} & \bar{Q}_{22} & \bar{Q}_{23} & 0 & 0 & 0 \\ \bar{Q}_{13} & \bar{Q}_{23} & \bar{Q}_{33} & 0 & 0 & 0 \\ 0 & 0 & 0 & \bar{Q}_{44} & \bar{Q}_{45} & 0 \\ 0 & 0 & 0 & \bar{Q}_{54} & \bar{Q}_{55} & 0 \\ 0 & 0 & 0 & 0 & 0 & \bar{Q}_{66} \end{bmatrix}^k \begin{Bmatrix} \epsilon_{\xi_1 \xi_1}^k \\ \epsilon_{\xi_2 \xi_2}^k \\ \epsilon_{\zeta \zeta}^k \\ \epsilon_{\xi_2 \zeta}^k \\ \epsilon_{\xi_1 \zeta}^k \\ \epsilon_{\xi_1 \xi_2}^k \end{Bmatrix}, \quad (1)$$

or $\{\sigma_{ij}\} = [\bar{Q}_{ij}]\{\epsilon_{ij}\}$,

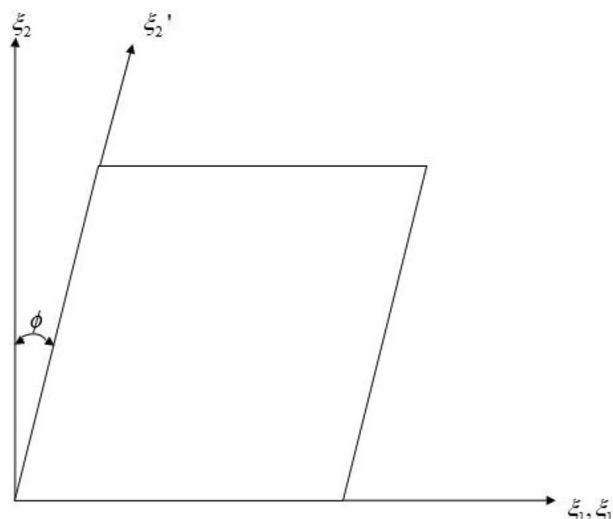


Fig. 2 Representation of the skew sandwich flat panel

where, $\{\sigma_{ij}\}$, $[\bar{Q}_{ij}]$ and $\{\epsilon_{ij}\}$ are the stress tensor, the reduced transformed stiffness matrix, and the strain tensor, respectively.

2.2 Displacement field

Now, the skew laminated sandwich structure model is derived mathematically via the proposed higher-order displacement kinematics [47] assuming the ESL theory including the stretching effect. The current kinematic model

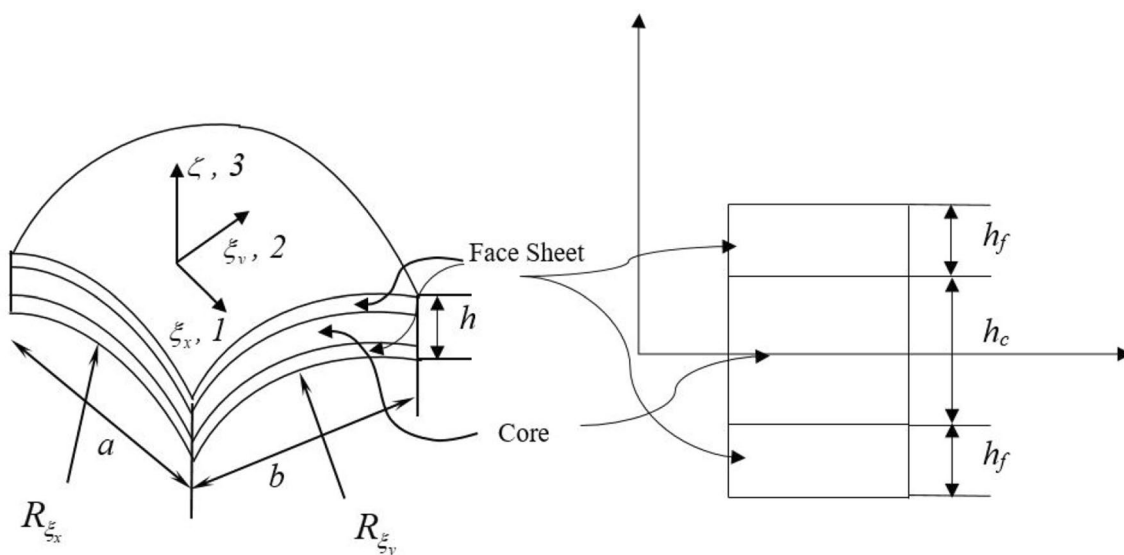


Fig. 1 Representation of the sandwich shell geometry

maintains the required order of equation for the proper strain and stress of the shell structure [49]. In addition, the displacement function maintains the parabolic shear stress distribution through the shell thickness and expressed as:

$$\left. \begin{aligned} \bar{u}(\xi_x, \xi_y, \zeta) &= u(\xi_x, \xi_y) + \zeta \theta_x(\xi_x, \xi_y) + \zeta^2 \lambda_x(\xi_x, \xi_y) + \zeta^3 \psi_x(\xi_x, \xi_y) \\ \bar{v}(\xi_x, \xi_y, \zeta) &= v(\xi_x, \xi_y) + \zeta \theta_y(\xi_x, \xi_y) + \zeta^2 \lambda_y(\xi_x, \xi_y) + \zeta^3 \psi_y(\xi_x, \xi_y) \\ \bar{w}(\xi_x, \xi_y, \zeta) &= w(\xi_x, \xi_y) + \zeta \theta_z(\xi_x, \xi_y) \end{aligned} \right\} \quad (2)$$

Here, the displacement of any general point within the panel is represented as $(\bar{u}, \bar{v}, \bar{w})$ whereas (u, v, w) signifies the mid-plane displacement of any particular point along the corresponding direction (ξ_x, ξ_y, ζ) , respectively. Similarly, the rotation of normal to the mid-plane and extension terms are denoted as θ_x, θ_y , and θ_z , respectively, along the corresponding direction. Few mathematical functions i.e. $\lambda_x, \lambda_y, \psi_x$ and ψ_y are defined at the mid-plane, showing the

higher-order terms introduced from Taylor's series expansion for the required parabolic distribution of shear stress across the thickness.

Now, the above Eq. (2) can be represented in the matrix form as:

$$\{\delta\} = [f] \{\delta_0\}, \quad (3)$$

where, $\{\delta\} = \{\bar{u} \ \bar{v} \ \bar{w}\}^T$, $[f]$ and $\{\delta_0\} = [u \ v \ w \ \theta_x \ \theta_y \ \theta_z \ \lambda_x \ \lambda_y \ \psi_x \ \psi_y]^T$ are the displacement field vector at any point, thickness coordinate matrix and displacement field vector within the mid-plane.

2.3 Strain–displacement relationship

The geometrical distortion of the sandwich composite shell panel including the large deformation has been mentioned using Green–Lagrange nonlinear strains as same as in [52] and elucidated as:

$$\left. \begin{aligned} \varepsilon_{\xi_x \xi_x} &= \left(\frac{\partial \bar{u}}{\partial \xi_x} + \frac{\bar{w}}{R_{\xi_x}} \right) + \frac{1}{2} \left[\left(\frac{\partial \bar{u}}{\partial \xi_x} + \frac{\bar{w}}{R_{\xi_x}} \right)^2 + \left(\frac{\partial \bar{v}}{\partial \xi_x} + \frac{\bar{w}}{R_{\xi_x \xi_y}} \right)^2 + \left(\frac{\partial \bar{w}}{\partial \xi_x} - \frac{\bar{u}}{R_{\xi_x}} \right)^2 \right] \\ \varepsilon_{\xi_y \xi_y} &= \left(\frac{\partial \bar{v}}{\partial \xi_y} + \frac{\bar{w}}{R_{\xi_y}} \right) + \frac{1}{2} \left[\left(\frac{\partial \bar{u}}{\partial \xi_y} + \frac{\bar{w}}{R_{\xi_x \xi_y}} \right)^2 + \left(\frac{\partial \bar{v}}{\partial \xi_y} + \frac{\bar{w}}{R_{\xi_x \xi_y}} \right)^2 + \left(\frac{\partial \bar{w}}{\partial \xi_y} - \frac{\bar{v}}{R_{\xi_y}} \right)^2 \right] \\ \varepsilon_{\zeta \zeta} &= \frac{\partial \bar{w}}{\partial \zeta} + \frac{1}{2} \left[\left(\frac{\partial \bar{u}}{\partial \zeta} \right)^2 + \left(\frac{\partial \bar{v}}{\partial \zeta} \right)^2 + \left(\frac{\partial \bar{w}}{\partial \zeta} \right)^2 \right] \\ \varepsilon_{\xi_x \zeta} &= \left(\frac{\partial \bar{v}}{\partial \zeta} + \frac{\partial \bar{w}}{\partial \xi_x} - \frac{\bar{v}}{R_{\xi_x}} \right) \\ &\quad + \left[\left(\frac{\partial \bar{u}}{\partial \zeta} \right) \left(\left(\frac{\partial \bar{u}}{\partial \xi_x} + \frac{\bar{w}}{R_{\xi_x \xi_y}} \right) + \left(\frac{\partial \bar{v}}{\partial \zeta} \right) \left(\left(\frac{\partial \bar{v}}{\partial \xi_x} + \frac{\bar{w}}{R_{\xi_x \xi_y}} \right) + \left(\frac{\partial \bar{w}}{\partial \zeta} \right) \left(\left(\frac{\partial \bar{w}}{\partial \xi_x} - \frac{\bar{v}}{R_{\xi_x}} \right) \right) \right) \right] \\ \varepsilon_{\xi_y \zeta} &= \left(\frac{\partial \bar{u}}{\partial \zeta} + \frac{\partial \bar{w}}{\partial \xi_y} - \frac{\bar{u}}{R_{\xi_y}} \right) \\ &\quad + \left[\left(\frac{\partial \bar{u}}{\partial \zeta} \right) \left(\left(\frac{\partial \bar{u}}{\partial \xi_x} + \frac{\bar{w}}{R_{\xi_x}} \right) + \left(\frac{\partial \bar{v}}{\partial \zeta} \right) \left(\left(\frac{\partial \bar{v}}{\partial \xi_x} + \frac{\bar{w}}{R_{\xi_x \xi_y}} \right) + \left(\frac{\partial \bar{w}}{\partial \zeta} \right) \left(\left(\frac{\partial \bar{w}}{\partial \xi_x} - \frac{\bar{u}}{R_{\xi_x}} \right) \right) \right) \right] \\ \varepsilon_{\xi_x \xi_y} &= \left(\frac{\partial \bar{u}}{\partial \xi_y} + \frac{\partial \bar{v}}{\partial \xi_x} + 2 \frac{\bar{w}}{R_{\xi_x \xi_y}} \right) \\ &\quad + \left[\left(\frac{\partial \bar{u}}{\partial \xi_x} + \frac{\bar{w}}{R_{\xi_x}} \right) \left(\frac{\partial \bar{u}}{\partial \xi_y} + \frac{\bar{w}}{R_{\xi_x \xi_y}} \right) + \left(\frac{\partial \bar{v}}{\partial \xi_x} + \frac{\bar{w}}{R_{\xi_x \xi_y}} \right) \left(\frac{\partial \bar{v}}{\partial \xi_y} + \frac{\bar{w}}{R_{\xi_y}} \right) + \left(\frac{\partial \bar{w}}{\partial \xi_x} - \frac{\bar{u}}{R_{\xi_x}} \right) \left(\frac{\partial \bar{w}}{\partial \xi_y} - \frac{\bar{v}}{R_{\xi_y}} \right) \right] \end{aligned} \right\} \quad (4)$$

or $\{\varepsilon\} = \{\varepsilon_l\} + \{\varepsilon_{nl}\}$.

Further, the detailed strain–displacement equation is expressed by incorporating the displacement functions (Eq. 2) in the corresponding strain Eq. (4) and conceded as:

the geometry has been modeled with the advent of FEM using a nine-noded isoparametric quadrilateral Lagrangian element and ten degrees of freedom per node for the accurate prediction of the final solution. The nodal displacement field

$$\begin{aligned}
 \{\varepsilon_l\} + \{\varepsilon_{nl}\} = & \underbrace{\begin{pmatrix} \varepsilon_{\xi_x \xi_x}^{l_0} \\ \varepsilon_{\xi_y \xi_y}^{l_0} \\ \varepsilon_{\xi_x \xi_y}^{l_0} \\ \varepsilon_{\xi_x \zeta}^{l_0} \\ \varepsilon_{\xi_y \zeta}^{l_0} \\ \varepsilon_{\xi_x \zeta}^{l_0} \\ \varepsilon_{\xi_x \zeta}^{l_0} \\ \varepsilon_{\xi_x \zeta}^{l_0} \end{pmatrix} + \zeta \underbrace{\begin{pmatrix} k_{\xi_x \xi_x}^{l_1} \\ k_{\xi_y \xi_y}^{l_1} \\ 0 \\ k_{\xi_y \zeta}^{l_1} \\ k_{\xi_x \zeta}^{l_1} \\ k_{\xi_x \zeta}^{l_1} \\ k_{\xi_x \zeta}^{l_1} \\ k_{\xi_x \zeta}^{l_1} \end{pmatrix}}_{\varepsilon_l} + \zeta^2 \underbrace{\begin{pmatrix} k_{\xi_x \xi_x}^{l_2} \\ k_{\xi_y \xi_y}^{l_2} \\ 0 \\ k_{\xi_y \zeta}^{l_2} \\ k_{\xi_x \zeta}^{l_2} \\ k_{\xi_x \zeta}^{l_2} \\ k_{\xi_x \zeta}^{l_2} \\ k_{\xi_x \zeta}^{l_2} \end{pmatrix}}_{\varepsilon_l} + \zeta^3 \underbrace{\begin{pmatrix} k_{\xi_x \xi_x}^{l_3} \\ k_{\xi_y \xi_y}^{l_3} \\ 0 \\ k_{\xi_y \zeta}^{l_3} \\ k_{\xi_x \zeta}^{l_3} \\ k_{\xi_x \zeta}^{l_3} \\ k_{\xi_x \zeta}^{l_3} \\ k_{\xi_x \zeta}^{l_3} \end{pmatrix}}_{\varepsilon_l} + \frac{1}{2} \underbrace{\begin{pmatrix} \varepsilon_{\xi_x \xi_x}^{nl_0} \\ \varepsilon_{\xi_y \xi_y}^{nl_0} \\ \varepsilon_{\xi_x \xi_y}^{nl_0} \\ 2\varepsilon_{\xi_y \zeta}^{nl_0} \\ 2\varepsilon_{\xi_x \zeta}^{nl_0} \\ 2\varepsilon_{\xi_x \zeta}^{nl_0} \\ 2\varepsilon_{\xi_x \zeta}^{nl_0} \\ 2\varepsilon_{\xi_x \zeta}^{nl_0} \end{pmatrix}}_{\varepsilon_{nl}} + \zeta \frac{1}{2} \underbrace{\begin{pmatrix} k_{\xi_x \xi_x}^{nl_1} \\ k_{\xi_y \xi_y}^{nl_1} \\ k_{\xi_x \xi_y}^{nl_1} \\ 2k_{\xi_y \zeta}^{nl_1} \\ 2k_{\xi_x \zeta}^{nl_1} \\ 2k_{\xi_x \zeta}^{nl_1} \\ 2k_{\xi_x \zeta}^{nl_1} \\ 2k_{\xi_x \zeta}^{nl_1} \end{pmatrix}}_{\varepsilon_{nl}} \\
 & + \zeta^2 \frac{1}{2} \underbrace{\begin{pmatrix} k_{\xi_x \xi_x}^{nl_2} \\ k_{\xi_y \xi_y}^{nl_2} \\ k_{\xi_x \xi_y}^{nl_2} \\ 2k_{\xi_y \zeta}^{nl_2} \\ 2k_{\xi_x \zeta}^{nl_2} \\ 2k_{\xi_x \zeta}^{nl_2} \\ 2k_{\xi_x \zeta}^{nl_2} \\ 2k_{\xi_x \zeta}^{nl_2} \end{pmatrix}}_{\varepsilon_{nl}} + \zeta^3 \frac{1}{2} \underbrace{\begin{pmatrix} k_{\xi_x \xi_x}^{nl_3} \\ k_{\xi_y \xi_y}^{nl_3} \\ k_{\xi_x \xi_y}^{nl_3} \\ 2k_{\xi_y \zeta}^{nl_3} \\ 2k_{\xi_x \zeta}^{nl_3} \\ 2k_{\xi_x \zeta}^{nl_3} \\ 2k_{\xi_x \zeta}^{nl_3} \\ 2k_{\xi_x \zeta}^{nl_3} \end{pmatrix}}_{\varepsilon_{nl}} + \zeta^4 \frac{1}{2} \underbrace{\begin{pmatrix} k_{\xi_x \xi_x}^{nl_4} \\ k_{\xi_y \xi_y}^{nl_4} \\ k_{\xi_x \xi_y}^{nl_4} \\ 2k_{\xi_y \zeta}^{nl_4} \\ 2k_{\xi_x \zeta}^{nl_4} \\ 2k_{\xi_x \zeta}^{nl_4} \\ 2k_{\xi_x \zeta}^{nl_4} \\ 2k_{\xi_x \zeta}^{nl_4} \end{pmatrix}}_{\varepsilon_{nl}} + \zeta^5 \frac{1}{2} \underbrace{\begin{pmatrix} k_{\xi_x \xi_x}^{nl_5} \\ k_{\xi_y \xi_y}^{nl_5} \\ k_{\xi_x \xi_y}^{nl_5} \\ 2k_{\xi_y \zeta}^{nl_5} \\ 2k_{\xi_x \zeta}^{nl_5} \\ 2k_{\xi_x \zeta}^{nl_5} \\ 2k_{\xi_x \zeta}^{nl_5} \\ 2k_{\xi_x \zeta}^{nl_5} \end{pmatrix}}_{\varepsilon_{nl}} + \zeta^6 \frac{1}{2} \underbrace{\begin{pmatrix} k_{\xi_x \xi_x}^{nl_6} \\ k_{\xi_y \xi_y}^{nl_6} \\ 0 \\ 0 \\ 0 \\ 0 \\ 2k_{\xi_x \zeta}^{nl_6} \\ 2k_{\xi_x \zeta}^{nl_6} \end{pmatrix}}_{\varepsilon_{nl}} \tag{5}
 \end{aligned}$$

or $\{\varepsilon_l\} + \{\varepsilon_{nl}\} = [T^l] \{\bar{\varepsilon}_l\} + [T^{nl}] \{\bar{\varepsilon}_{nl}\}$,

where $[T^l]$ and $[T^{nl}]$ are the thickness co-ordinate matrix associated with the linear and nonlinear mid-plane strains, respectively, and the individual strain values can be referred in the reference [48]. In addition, the mid-plane linear and nonlinear strain vectors are represented as $\{\bar{\varepsilon}_l\}$ and $\{\bar{\varepsilon}_{nl}\}$, respectively.

2.4 Nonlinear finite element scheme

The FEM has proved to provide an accurate numerical solution for the complex engineering problems with minimal error. Moreover, the composite modeling and analysis of the layered composite become a nontrivial type for the larger number of unknowns due to the increase in layer number. In addition, the presently developed numerical model is associated with complexities associated with the sandwich construction including the variable material properties. Hence,

expressions are rewritten using the FEM steps and conceded to the following form:

$$\{\delta_0^*\} = [u \ v \ w \ \theta_x \ \theta_y \ \theta_z \ \lambda_x \ \lambda_y \ \psi_x \ \psi_y]^T = \sum_{i=1}^9 [N_i] \{\delta_{0i}\} \tag{6}$$

Here, the interpolation function (shape function) termed as, $[N_i]$ and the displacement field vector for the i th node is denoted as $\{\delta_{0i}\}$. The mathematical expressions of the nodal points are generally replicate the physical characteristics and the shape functions of the current element can be seen in [51].

Now, the mid-plane strain vector can be written as:

$$\{\varepsilon\}_i = [B_i] \{\delta_{0i}^*\}, \tag{7}$$

where, $[B_i]$ is the strain displacement relation matrix.

Further, the transformed nodal co-ordinates in the Cartesian coordinate system are defined using the transformation matrix $[T_3]$ as:

$$\{\delta_0^{**}\} = [T_S]\{\delta_0^*\}, \tag{8}$$

where,

where, $\{\epsilon_l\}_i = [B_l]_i\{\delta_0^{**}\}$ and $\{\epsilon_{nl}\}_i = \frac{1}{2}[B_{nl}]_i\{\delta_0^{**}\} = \frac{1}{2}[A]_i[G]_i\{\delta_0^{**}\}$. $[B_l]$ is linear strain–displacement matrix

$$[T_S] = \begin{bmatrix} \cos \phi & -\sin \phi & 0 & 0 & 0 & 0 & 0 & 0 & 0 & 0 \\ \sin \phi & \cos \phi & 0 & 0 & 0 & 0 & 0 & 0 & 0 & 0 \\ 0 & 0 & 1 & 0 & 0 & 0 & 0 & 0 & 0 & 0 \\ 0 & 0 & 0 & \cos \phi & -\sin \phi & 0 & 0 & 0 & 0 & 0 \\ 0 & 0 & 0 & \sin \phi & \cos \phi & 0 & 0 & 0 & 0 & 0 \\ 0 & 0 & 0 & 0 & 0 & 1 & 0 & 0 & 0 & 0 \\ 0 & 0 & 0 & 0 & 0 & 0 & \cos \phi & -\sin \phi & 0 & 0 \\ 0 & 0 & 0 & 0 & 0 & 0 & \sin \phi & \cos \phi & 0 & 0 \\ 0 & 0 & 0 & 0 & 0 & 0 & 0 & 0 & \cos \phi & -\sin \phi \\ 0 & 0 & 0 & 0 & 0 & 0 & 0 & 0 & \sin \phi & \cos \phi \end{bmatrix}.$$

2.5 Strain energy of the panel

In general, for any laminated sandwich composite shell panel, the strain energy (U) can be expressed in the following form [52]:

$$U = \frac{1}{2} \int_v \{\epsilon\}_i^T \{\sigma_i\} dV. \tag{9}$$

By substituting the total stress tensors and the strain vectors from the Eqs. (1) and (5) into the energy Eq. (9) and the final form of the energy functional of the panel configuration can be elucidated as:

whereas $[A]$ is the function of the displacement associated with nonlinear strain matrix. Additionally, $[G]$ is as same as the linear strain–displacement matrix. The nonlinear strain terms including the detailed individual coefficients can be seen in [48].

2.6 Work done of the panel

The total work done expression due to the externally applied distributed mechanical transverse static load ‘ q ’ on a generalized structure or the current sandwich panel and it can be interpreted as in [52]:

$$\left. \begin{aligned} U &= \frac{1}{2} \int_v \{\epsilon\}_i^T [\bar{Q}] \{\epsilon\}_i dV \\ &= \frac{1}{2} \iiint \{\epsilon_l + \epsilon_{nl}\}^T [\bar{Q}] \{\epsilon_l + \epsilon_{nl}\} d\xi_x d\xi_y d\xi_z \\ &= \frac{1}{2} \int_A \left(\{\epsilon_l\}_i^T [D_1] \{\epsilon_l\}_i + \frac{1}{2} \{\epsilon_l\}_i^T [D_2] \{\epsilon_{nl}\}_i + \frac{1}{2} \{\epsilon_{nl}\}_i^T [D_3] \{\epsilon_l\}_i + \frac{1}{2} \{\epsilon_{nl}\}_i^T [D_4] \{\epsilon_{nl}\}_i \right) dA \end{aligned} \right\} \tag{10}$$

where,

$$\begin{aligned} [D_1] &= \sum_{k=1}^N \int_{\zeta_{k-1}}^{\zeta_k} [T^l]^T [\bar{Q}] [T^l] d\zeta, & [D_2] &= \sum_{k=1}^N \int_{\zeta_{k-1}}^{\zeta_k} [T^l]^T [\bar{Q}] [T^{nl}] d\zeta, \\ [D_3] &= \sum_{k=1}^N \int_{\zeta_{k-1}}^{\zeta_k} [T^{nl}]^T [\bar{Q}] [T^l] d\zeta, & [D_4] &= \sum_{k=1}^N \int_{\zeta_{k-1}}^{\zeta_k} [T^{nl}]^T [\bar{Q}] [T^{nl}] d\zeta, \end{aligned}$$

Now, substituting Eq. (7) into Eq. (10) and the expression for the strain energy conceded:

$$W = \int_A \{\delta_0^{**}\}^T q dA. \tag{12}$$

$$U = \frac{1}{2} \int_A \left(\{\delta_0^*\}^T [B_l]_i^T [D_1] [B_l]_i \{\delta_0^*\} + \frac{1}{2} \{\delta_0^*\}^T [B_l]_i^T [D_2] [A]_i [G]_i \{\delta_0^*\} + \frac{1}{2} \{\delta_0^*\}^T [G]_i^T [A]_i^T [D_3] [A]_i [B_l]_i \{\delta_0^*\} + \frac{1}{2} \{\delta_0^*\}^T [G]_i^T [A]_i^T [D_4] [A]_i [G]_i \{\delta_0^*\} \right) dA \tag{11}$$

2.7 Governing equation and solution approach

Now, the final form of the governing equation of the sandwich structural panel including the large deformation behaviour is obtained by minimising the total energy functionals and denoted as in [52]:

$$\delta\Pi = 0 \tag{13}$$

where, $\Pi = (U - W)$.

Subsequently, Eqs. (9)–(12) are inducted into Eq. (13) in association with the FE approximation as stated in Eq. (6). The final system equilibrium equation will be turned into the following form:

$$[K]\{\delta_0^{**}\} = \{q\} \text{ or } [K_l + K_{nl}]\{\delta_0^{**}\} = \{q\}, \tag{14}$$

where, $[K_l]$ and $[K_{nl}]$ are the global stiffness matrices for the structural component considering the linear and the nonlinear strain expression, respectively.

The desired deflection (linear or nonlinear) values of the sandwich structural panel have been obtained by solving the derived final Eq. (14) with the help of a robust solution technique (the direct iterative method). Further, the nonlinear deflection parameter of the sandwich panel is computed by setting the necessary tolerance $\left(\sqrt{(\bar{\delta}_n - \bar{\delta}_{n-1})^2 / (\bar{\delta}_n)^2} \leq \varepsilon\right)$

limit ($\approx 10^{-3}$) between two successive iterations. The details steps regarding the implementation of nonlinear solution process can be seen from the source [49].

3 Results and discussions

To establish the robustness of the current FEM solution, the convergence rate is evaluated for different mesh division (coarse to fine mesh) as well as the final responses (linear and nonlinear deflection) are compared with the published results. The necessary results are evaluated computationally through a customized computer code (MATLAB environment) using the current higher-order nonlinear FE model of the sandwich skew panel. To avoid the locking phenomena, a selective integration scheme has been employed, i.e., reduced integration for the transverse shear cases and full integration for the all other stress. In addition, the computation has been carried out for the combination of different end support conditions and provided in Table 1. Three different set of materials have been used in the current study named as M1, M2 and M3 and the details are provided below. The values are not altered in any case if not stated otherwise.

3.1 Material 1 (M1) [40]

Face : $E_1/E_2 = 10, G_{12} = G_{13} = 0.33E_2, G_{23} = 0.2E_2, \nu_{12} = 0.22,$

Core : $E_1 = 0.04E_2, G_{12} = 0.016E_2, G_{13} = G_{23} = 0.06E_2, \nu_{12} = 0.25.$

Table 1 End support conditions

Condition	at $\xi_x = 0, a$	at $\xi_y = 0, b$
Simply-supported (S)	$\left. \begin{matrix} v \\ w \\ \theta_y \\ \theta_z \\ \lambda_y \\ \psi_y \end{matrix} \right\} = 0$	$\left. \begin{matrix} u \\ w \\ \theta_x \\ \theta_z \\ \lambda_x \\ \psi_x \end{matrix} \right\} = 0$
Clamped (C)	$u = v = w = \theta_x = \theta_y = \theta_z = \lambda_x = \lambda_y = \psi_x = \psi_y = 0$	

3.2 Material 2 (M2) [28]

Face : $E_1 = 25E, E_2 = E, G_{12} = G_{13} = 0.5E, G_{23} = 0.2E, \nu_{12} = 0.25,$

Core : $E_1 = 0.04E, E_2 = 0.04E, G_{12} = 0.016E, G_{13} = G_{23} = 0.06E, \nu_{12} = 0.25.$

3.3 Material 3 (M3) [54]

Face : $E_1 = 172.5 \text{ GPa}, E_2 = E_3 = 6.89 \text{ GPa}, G_{12} = G_{13} = 3.45 \text{ GPa}, G_{23} = 1.378 \text{ GPa}, \nu_{12} = \nu_{13} = \nu_{23} = 0.25,$

Core : $E_1 = E_2 = 0.276 \text{ GPa}, E_3 = 3.45 \text{ GPa}, G_{12} = 0.1104 \text{ GPa}, G_{13} = G_{23} = 0.414 \text{ GPa}, \nu_{12} = 0.25\nu_{13} = \nu_{23} = \nu_{12}.$

$$Q = q_0 a^4 / E_{xz} h^4; W^* = W_0 / h,$$

$$\bar{\sigma}_{\xi_x \xi_x}(a/2, b/2, \zeta) = \sigma_{\xi_x \xi_x} h^2 / (qa^2); \bar{\sigma}_{\xi_y \xi_y}(a/2, b/2, \zeta) = \sigma_{\xi_y \xi_y} h^2 / (qa^2),$$

$$\bar{\tau}_{\xi_x \zeta}(0, b/2, \zeta) = \tau_{\xi_x \zeta} h / (qa); \bar{\tau}_{\xi_y \zeta}(a/2, 0, \zeta) = \tau_{\xi_y \zeta} h / (qa);$$

$$\bar{\tau}_{\xi_x \xi_y}(a, b, \zeta) = \tau_{\xi_x \xi_y} h^2 / (qa^2).$$

Finally, different parametric studies have been carried out to assess the static deflection values of the skew sandwich structural components including the variation of geometries.

As a first step, a convergence study (different mesh division) is carried out for an example of all edges clamped (CCCC) ($0^\circ/90^\circ/\text{Core}/90^\circ/0^\circ$) skew ($\phi = 45^\circ$) sandwich flat panel and the corresponding values presented in Fig. 3. The results are obtained for the various loading parameter (Q) by utilizing the necessary input parameter (material properties [1] and geometry related data) i.e. side-to-thickness ratio ($a/h = 40$) and core-to-face thickness ratio ($h_c/h_f = 8$). It is clearly understood from the figure that the results are converging well with the mesh refinement and the current (6×6) mesh size is capable of calculating the nonlinear

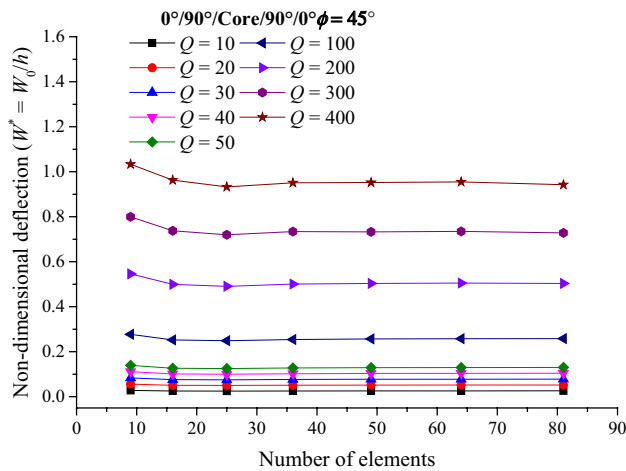
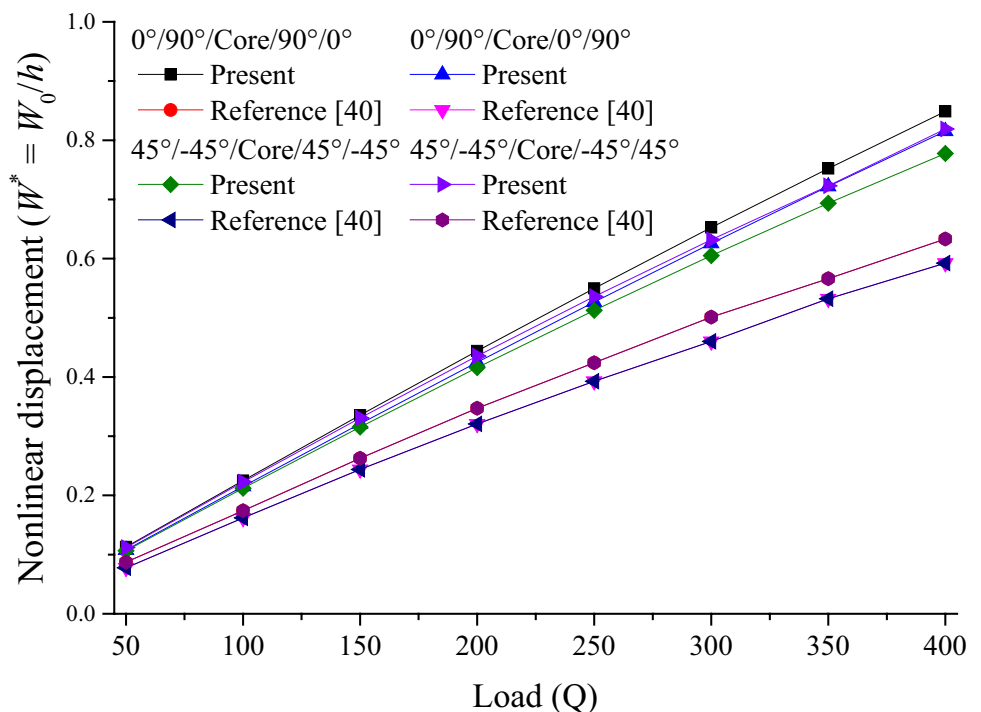


Fig. 3 Convergence study of non-dimensional deflection ($W^* = W_0/h$) of clamped ($0^\circ/90^\circ/\text{Core}/0^\circ/90^\circ$) skew ($\phi = 45^\circ$) sandwich flat panels ($al/h = 40, h_c/h_f = 8$)

static responses with satisfactory exactitude for further computational purpose.

Subsequently, the validity of the current numerical model is checked by solving a new example taking the input parameter (the material and geometrical parameters) as same as the convergence case and plotted in Fig. 4. Additionally, the responses are also obtained for different lamination schemes ($0^\circ/90^\circ/\text{Core}/90^\circ/0^\circ, 0^\circ/90^\circ/\text{Core}/0^\circ/90^\circ, 45^\circ/-45^\circ/\text{Core}/-45^\circ/45^\circ$ and $45^\circ/-45^\circ/\text{Core}/45^\circ/-45^\circ$) of the composite face sheets. The final values are compared with the

Fig. 4 Non-dimensional deflection ($W^* = W_0/h$) of clamped skew ($\phi = 45^\circ$) sandwich flat/curved panels ($al/h = 40, h_c/h_f = 8$)



reference [40] which shows a good agreement with the small deviation. However, the major reason of the differences is strain–displacement relation, i.e., Green–Lagrange strain is used in a present case whereas reference used the von-Karman type of strain field. Additionally, the said numerical model first time includes all of the nonlinear higher-order terms for the skew sandwich structure to arrest the exact flexure.

Moreover, to show the model accuracy another example is solved to validate the deflection and normal stress values with available benchmark solutions i.e. 3D elasticity result. The values are computed using the material properties (M2) and the geometrical parameters as same as [28].

For the computational purpose, a square simply-supported sandwich plate under uniformly distributed load with two different lamination schemes ($0^\circ/90^\circ/\text{C}/0^\circ/90^\circ$ and $30^\circ/-30^\circ/\text{C}/30^\circ/-30^\circ$) and two side-to-thickness ratios ($al/h = 10$ and 20) is considered and the results are presented in Table 2. It is observed from the table that the calculated values are in good agreement with the RHSDT solution including the results computed via 3D elasticity theory. Here, the normalized non-dimensional values of the central deflections and the in-plane normal stress at the centre of the panel are obtained using the similar formula as in the reference ($\bar{W} = 100wEh^3/(qa^4)$ and $\bar{\sigma}_{\xi_x\xi_x} = \sigma_{\xi_x\xi_x}h^2/(qa^2)$). The small deviation in the present and the reference results may be due to the different kinematic models and types of element. It is important to note that the current solutions are obtained by utilizing the higher-order displacement kinematics with ten DOF and 2-D nine-noded isoparametric

Table 2 Deflection and normal stress comparison for a simply-supported square sandwich plate under uniformly distributed load

Lamination scheme	alh	Theory	Deflection (\bar{W})	Normal stress ($\bar{\sigma}_{\xi_x, \xi_x}$)
(0°/90°/C/0°/90°)	10	Present HSDT	2.4588	1.7923
		RHSDT [28]	2.6296	1.6249
		3-D Elasticity [53]	2.6384	1.6214
	20	Present HSDT	1.6273	1.7022
		RHSDT [28]	1.7114	1.5988
		3-D Elasticity [53]	1.7116	1.5931
(30°/-30°/C/30°/-30°)	10	Present HSDT	2.0199	0.8103
		RHSDT [28]	2.2237	0.8882
	20	Present HSDT	1.1327	0.7707
		RHSDT [28]	1.2362	0.7653

Table 3 Maximum stresses of simply-supported square symmetric (0°/C/0°) sandwich plate under sinusoidal transverse load

alh	Model	$\bar{\sigma}_{\xi_x, \xi_x} \left(\frac{a}{2}, \frac{b}{2}, \frac{h}{2} \right)$	$\bar{\sigma}_{\xi_y, \xi_y} \left(\frac{a}{2}, \frac{b}{2}, \frac{h}{6} \right)$	$\bar{\tau}_{\xi_x, \xi_y} \left(0, 0, \frac{h}{2} \right)$	$\bar{\tau}_{\xi_x, \xi_z} \left(0, \frac{b}{2}, 0 \right)$	$\bar{\tau}_{\xi_y, \xi_z} \left(\frac{a}{2}, 0, 0 \right)$
4	Present	1.509	0.2457	-0.1378	0.2256	0.0961
	Kant et al. [54]	1.556	0.259	-0.144	0.239	0.107
	Pagano [55]	1.556	0.259	-0.144	0.239	0.107
	Pandya and Kant [56]	1.523	0.241	-0.142	0.275	-
	Wu and Kuo [57]	1.548	0.249	-	-	-0.134
	Ramtekkar et al. [58]	1.57	0.26	-	0.237	0.104
10	Present	1.1563	0.0912	-0.0679	0.2812	0.0506
	Kant et al. [54]	1.153	0.11	-0.0707	0.3	0.0527
	Pagano [55]	1.153	0.11	-0.071	0.3	0.053
	Pandya and Kant [56]	1.166	0.105	-0.069	0.34	-
	Wu and Kuo [57]	1.21	0.111	-0.071	0.324	-
	Ramtekkar et al. [58]	1.159	0.111	-0.071	0.303	0.055
20	Present	1.1154	0.0621	-0.0497	0.3011	0.0397
	Kant et al. [54]	1.11	0.07	-0.051	0.317	0.036
	Pagano [55]	1.11	0.07	-0.051	0.317	0.036
	Wu and Kuo [57]	1.173	0.072	0.052	0.353	-
	Ramtekkar et al. [58]	1.115	0.07	-0.051	0.317	0.036

quadrilateral Lagrangian element whereas the refined higher-order kinematics with seven DOF including the six-noded triangular element adopted in the reference [28].

Further, the stresses (in-plane and out of plane) are evaluated for the three-layered (0°/C/0°) square simply-supported sandwich plate structure under the sinusoidal loading. The responses are compared with available data solved via different techniques (semi-analytical model [54]; elasticity solution [55]; FEM and HSDT with 5 DOF [56]; mixed FEM [57, 58] with 11 and 6 DOF) and presented in Table 3. The material and geometrical parameter are considered same as reference [54]. The sinusoidal load is considered according to the formulae: $Q = q_0 \sin \left(\frac{\pi \xi_x}{a} \right) \sin \left(\frac{\pi \xi_y}{b} \right)$. The validation study indicates that the present responses are close to

the reference values. Additionally, the small deviation between the present and the reference results may be due to the difference kinematic models including the numbers of DOF at each node.

4 Numerical examples

After the required conformation test of the present higher-order numerical model of the skew sandwich panel structure, it is extended to examine the substantial effect different associated design parameters on the transverse deflection values including the geometries (Cyl, Elpt, Sph, Hyp and FP) and full geometrical nonlinearity. It is important to mention

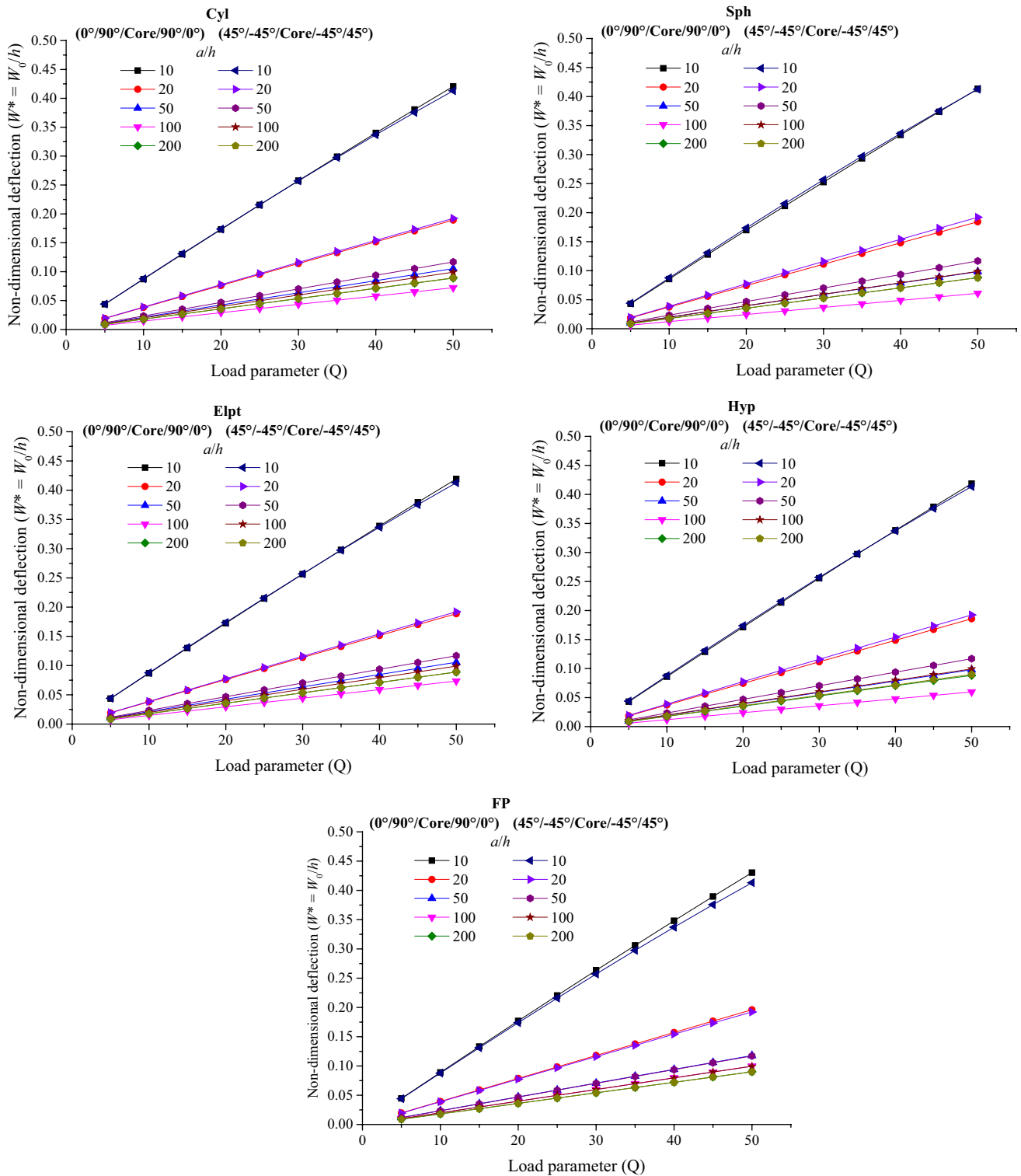


Fig. 5 Effect of side-to-thickness ratio (a/h) on non-dimensional deflection ($W^* = W_0/h$) of clamped skew ($\phi = 45^\circ$) sandwich flat/curved panels ($R/a = 50, h_c/h_f = 8$)

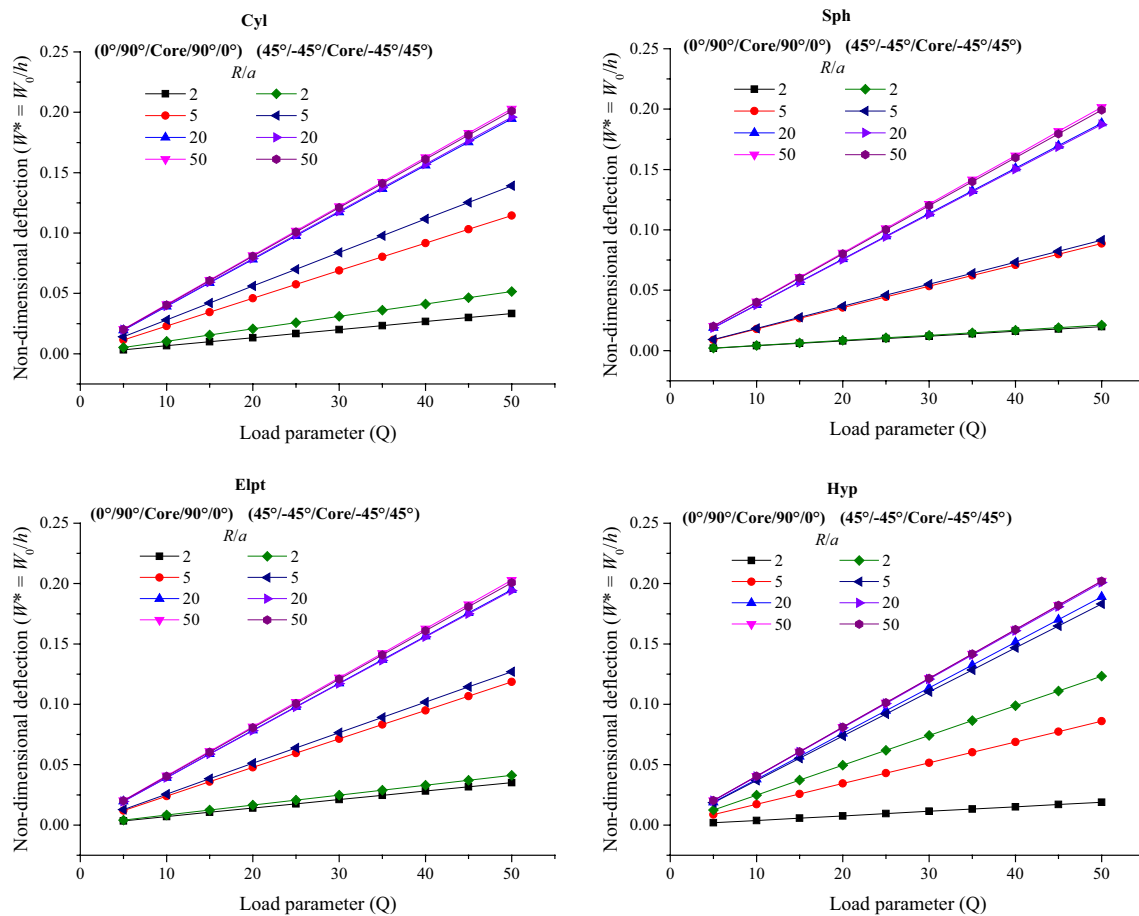


Fig. 6 Effect of curvature ratio (R/a) on non-dimensional deflection ($W^* = W_0/h$) of clamped skew ($\phi = 30^\circ$) sandwich curved panels ($a/h = 100$, $h_c/h_f = 8$)

that the material property M1 is considered further for new numerical illustration else stated otherwise.

4.1 Effect of side-to-thickness ratio (a/h)

In the present numerical example, the non-dimensional deflections are obtained for the clamped skew ($\phi = 45^\circ$) flat/curved shell panels using the earlier defined material parameters and presented in Fig. 5. For the computation purpose, the two lamination schemes ($0^\circ/90^\circ/\text{Core}/90^\circ/0^\circ$ and $45^\circ/-45^\circ/\text{Core}/-45^\circ/45^\circ$) and the geometrical parameters $a/h = 10, 20, 50, 100$ and 200 , $R/a = 50$ and $h_c/h_f = 8$ are considered. From the figure, it is observed that the non-dimensional deflection values are decreasing while the a/h values increase. The deflection results indicate the higher values for the angle-ply ($45^\circ/-45^\circ/\text{Core}/-45^\circ/45^\circ$) sandwich panel in comparison to the cross-ply ($0^\circ/90^\circ/\text{Core}/90^\circ/0^\circ$) case. In addition, the deflection values are following an increasing trend when the load parameter (Q) values increase. The

deflection values decrease as the geometry of the structure changes from, Hyp, Cyl, Elpt, Sph, and FP.

4.2 Effect of curvature ratio (R/a)

To study the influence of the curvature ratio, the non-dimensional deflection parameter of the skew ($\phi = 30^\circ$) clamped curved shell panel example is solved. The results are computed using the M1 material parameter and presented in Fig. 6. Here, the responses also examined for two lamination schemes i.e. the cross-ply and angle-ply ($0^\circ/90^\circ/\text{Core}/90^\circ/0^\circ$ and $45^\circ/-45^\circ/\text{Core}/-45^\circ/45^\circ$) cases. The results are obtained for four curvature ratios ($R/a = 2, 5, 20$ and 50) by setting other geometrical parameters i.e. $a/h = 100$ and $h_c/h_f = 8$. The obtained results clearly indicate that the non-dimensional deflection values are increasing when the load parameter (Q) and curvature ratio (R/a) values increase. It is because of the well-known fact that the structural stiffness reduces when curvature value increase. In addition, the

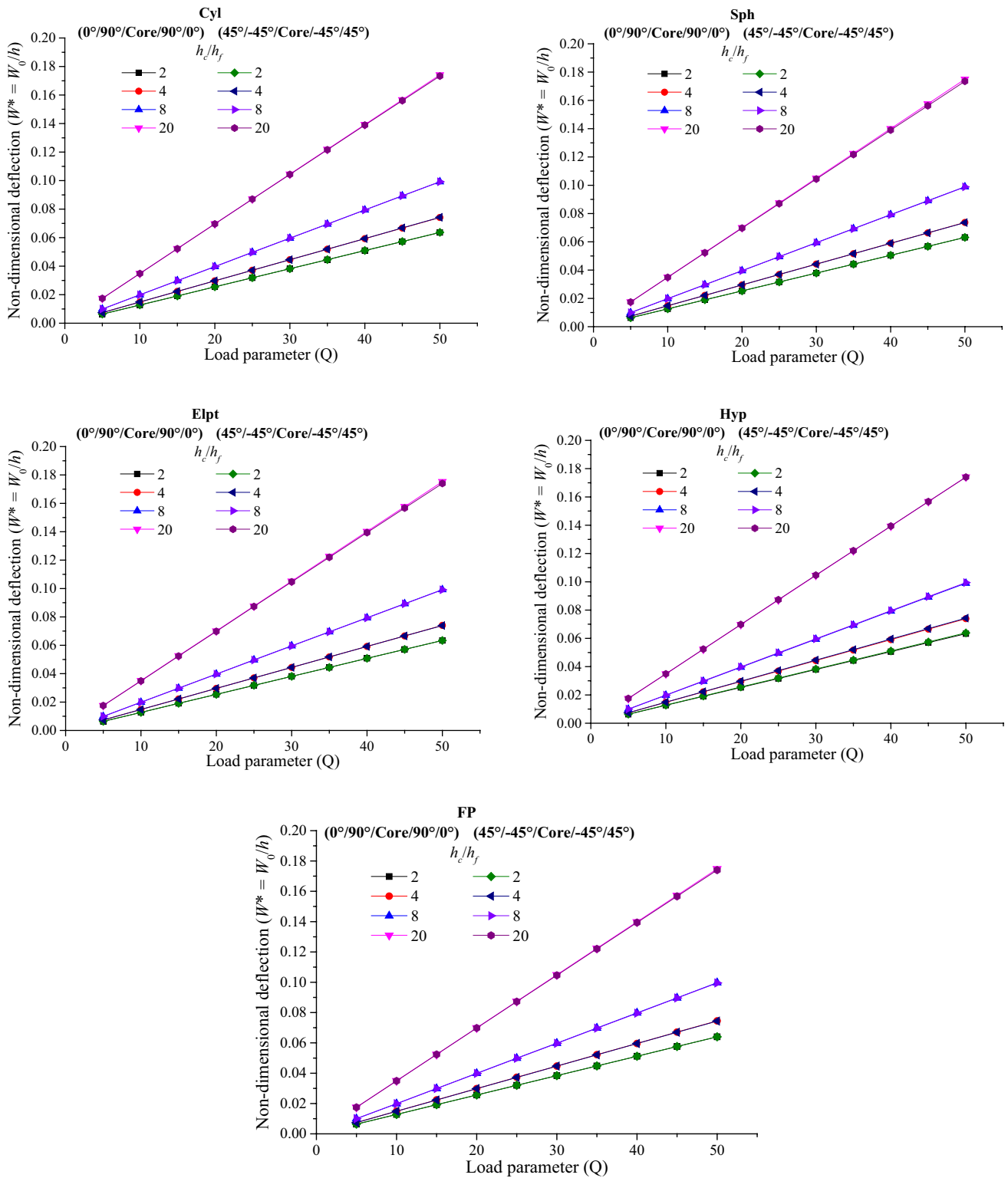


Fig. 7 Effect of core-to-face thickness ratio (h_c/h_f) on non-dimensional deflection ($W^* = W_0/h$) of clamped skew ($\phi=45^\circ$) sandwich curved panels ($ah=100, R/a=50$)

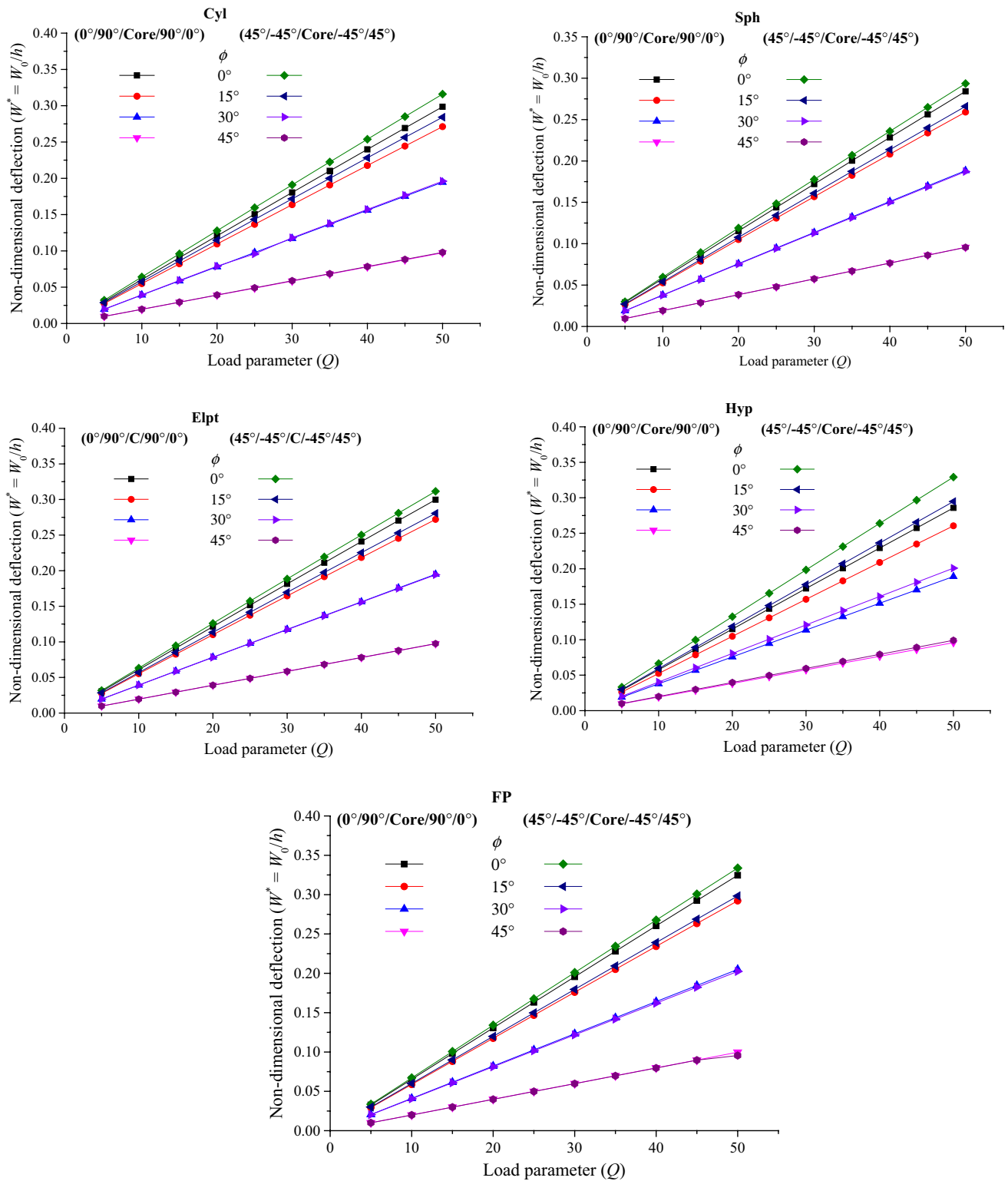


Fig. 8 Effect of skew angle on non-dimensional deflection ($W^* = W_0/h$) of clamped sandwich curved panels ($a/h = 100, R/a = 20, h_c/h_f = 8$)

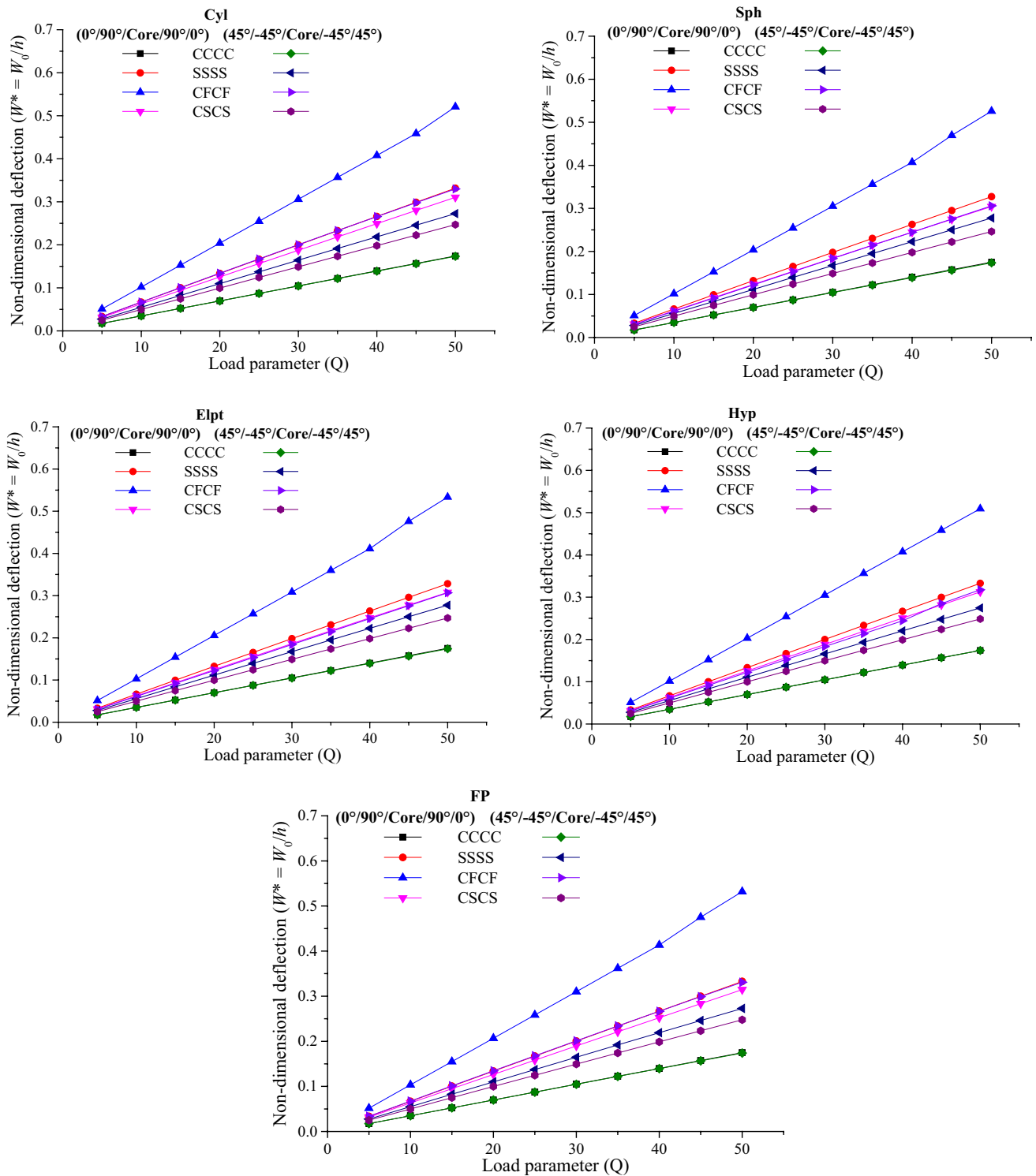


Fig. 9 Effect of support conditions on non-dimensional deflection ($W^* = W_0/h$) of skew ($\phi = 45^\circ$) sandwich curved panels ($a/h = 100$, $R/a = 50$, $h_c/h_t = 20$)

results show that the deflection values are higher for the angle-ply ($45^\circ/-45^\circ/\text{Core}/-45^\circ/45^\circ$) sandwich structure in comparison to the cross-ply ($0^\circ/90^\circ/\text{Core}/90^\circ/0^\circ$) panel

as in the earlier case. The deflection values are following a declining trend while the geometrical configuration changes from, Cyl, Hyp, Elpt and Sph panel.

Table 4 Deflection and normal stress of a simply-supported ($0^\circ/90^\circ/C/0^\circ/90^\circ$) square sandwich shell panels under uniformly distributed load ($h_c/h_f = 8$)

a/h	Theory	R/a							
		Deflection (\bar{W})				Normal stress ($\bar{\sigma}_{\epsilon_x \epsilon_x}$)			
		5	10	20	50	5	10	20	50
5	FP	5.772	5.772	5.772	5.772	2.1955	2.1955	2.1955	2.1955
	Cyl	5.7703	5.7708	5.7713	5.7717	0.7489	1.4742	1.8353	2.0516
	Sph	5.7236	5.7596	5.7688	5.7714	0.779	1.4892	1.8434	2.055
	Hyp	5.8201	5.7827	5.774	5.772	0.7215	1.46	1.8275	2.0482
	Elpt	5.7465	5.7651	5.77	5.7715	0.7636	1.4816	1.8393	2.0533
10	FP	2.4588	2.4588	2.4588	2.4588	1.7923	1.7923	1.7923	1.7923
	Cyl	2.4516	2.4569	2.4582	2.4586	0.5666	1.1814	1.4875	1.6705
	Sph	2.4107	2.4465	2.4557	2.4582	0.5852	1.1908	1.4932	1.6732
	Hyp	2.48	2.4639	2.46	2.4589	0.5452	1.1705	1.4813	1.6678
	Elpt	2.4327	2.4521	2.457	2.4585	0.5763	1.1862	1.4904	1.6719
15	FP	1.8429	1.8429	1.8429	1.8429	1.7241	1.7241	1.7241	1.7241
	Cyl	1.8292	1.8394	1.842	1.8427	0.3527	1.0398	1.3828	1.5878
	Sph	1.7749	1.8254	1.8385	1.8422	0.3714	1.0473	1.388	1.5905
	Hyp	1.8587	1.8468	1.8438	1.843	0.3278	1.0283	1.3762	1.5849
	Elpt	1.8049	1.8332	1.8404	1.8425	0.3628	1.044	1.3855	1.5892
20	FP	1.6273	1.6273	1.6273	1.6273	1.7022	1.7022	1.7022	1.7022
	Cyl	1.6051	1.6217	1.6259	1.6271	0.0945	0.8979	1.301	1.5421
	Sph	1.5297	1.6018	1.6209	1.6263	0.1219	0.9045	1.3061	1.545
	Hyp	1.6411	1.6307	1.6282	1.6275	0.0613	0.8848	1.2936	1.5387
	Elpt	1.5717	1.6131	1.6237	1.6267	0.109	0.902	1.3038	1.5436

4.3 Effect of core-to-face thickness ratio (h_c/h_f)

The core-to-face thickness ratio (h_c/h_f) have significant influence on the nonlinear deflection parameter of the sandwich structure. In this regard, an example is solved for a thin ($a/h = 100$) clamped skew ($\phi = 45^\circ$) shell structural panel ($R/a = 50$) of two lamination ($0^\circ/90^\circ/\text{Core}/90^\circ/0^\circ$ and $45^\circ/-45^\circ/\text{Core}/-45^\circ/45^\circ$) schemes. The central deflection are obtained for four different h_c/h_f (2, 4, 8 and 20) values and presented in Fig. 7. The results clearly indicate that the non-dimensional deflection values are increasing while the h_c/h_f and the load parameters (Q) increase. In addition, the results show that the deflection values are following a similar type of trend as in the earlier case for the lamination scheme i.e. higher for angle-ply ($45^\circ/-45^\circ/\text{Core}/-45^\circ/45^\circ$) in comparison to the cross-ply ($0^\circ/90^\circ/\text{Core}/90^\circ/0^\circ$) sandwich panel. In addition, interesting to note that the deflections are higher and lower for the Hyp and FP sandwich panel structure.

4.4 Effect of skew angle (ϕ)

It is well known that the skew angle (ϕ) affects the structural responses greatly. Hence, an example is solved to study the effect of different values of the skew angles ($\phi = 0^\circ, 15^\circ, 30^\circ$ and 45°) on the non-dimensional deflection values of the

clamped shell panel (flat/curved) structure. The responses are obtained using the defined elastic properties and reported in Fig. 8. In this example, two different lamination schemes ($0^\circ/90^\circ/\text{Core}/90^\circ/0^\circ$ and $45^\circ/-45^\circ/\text{Core}/-45^\circ/45^\circ$) for the face sheets are adopted including the necessary geometrical parameters as: $a/h = 100$, $R/a = 20$ and $h_c/h_f = 8$. From the computed results, it is easy to understand that the non-dimensional deflection values are decreasing while the skew angle (ϕ) increases from 0° to 45° . However, the responses follow an increasing slope when the load parameter (Q) increase. Further, it is significant to note that the central point deflection values of the angle-ply laminations are higher in comparison to the cross-ply cases. In addition, the results indicate that the deflection values follow a declining trend when the geometry of the panel changes from, FP, Hyp, Cyl, Elpt and Sph i.e., the structural panel become stiffer as the curvature values increase.

4.5 Effect of support conditions

The effect of end conditions on the static responses are investigated and presented in Fig. 9. For the computational purpose, the skew ($\phi = 45^\circ$) flat/curved shell panel problem is solved including different end support conditions i.e., all edges clamped (CCCC), all edges simply-supported (SSSS), two opposite edges clamped and free (CFCF), two opposite

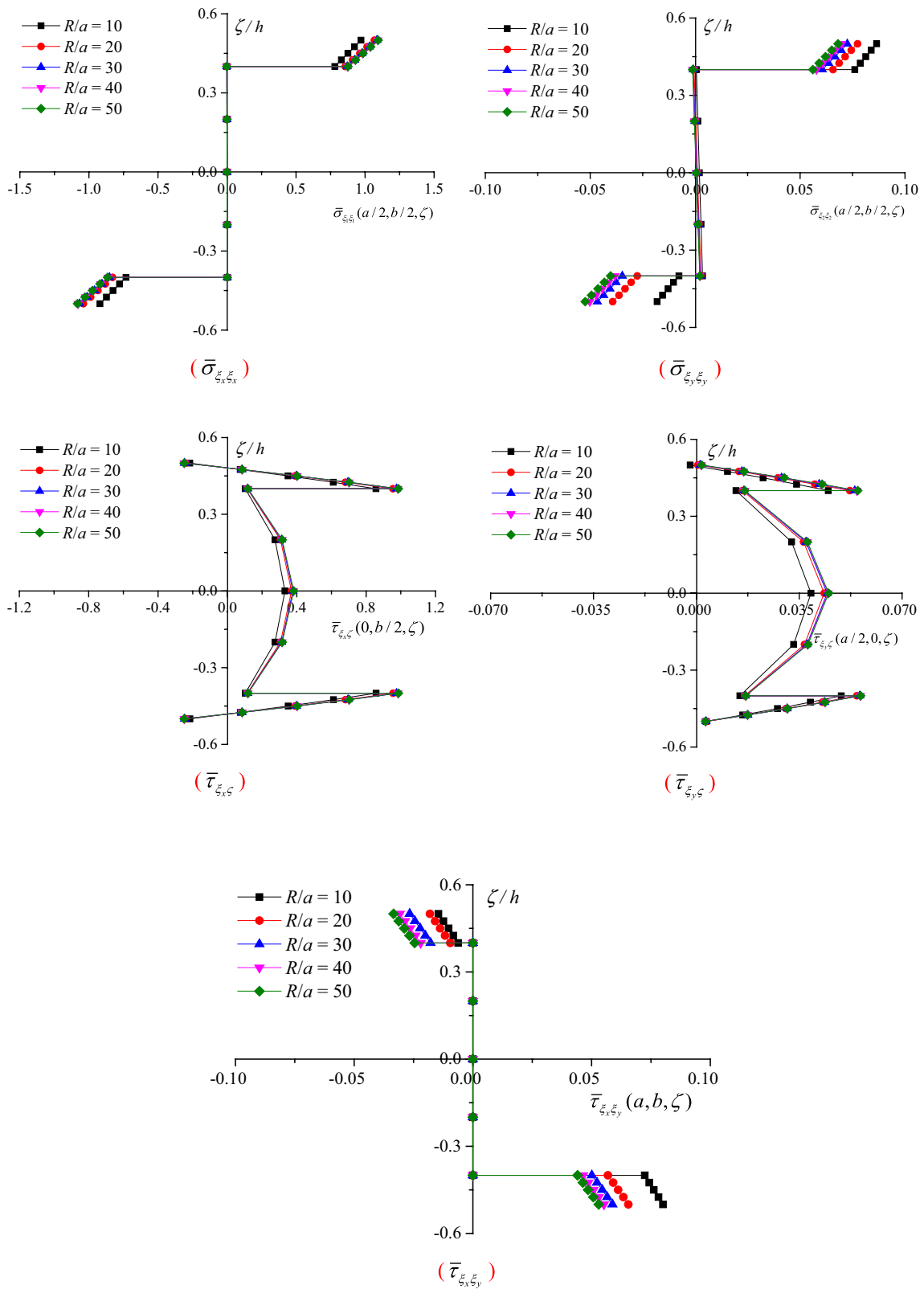


Fig. 10 Distribution of stresses over the thickness of a simply-supported ($0^\circ/C/0^\circ$) square sandwich spherical shell panel under sinusoidal transverse load ($h_c/h_f = 8, ah = 80$)

edges clamped and simply-supported (CSCS) along with the two lamination schemes i.e. $(0^\circ/90^\circ/\text{Core}/90^\circ/0^\circ)$ and $45^\circ/-45^\circ/\text{Core}/-45^\circ/45^\circ)$ and other geometrical parameters are: $a/h = 100$, $R/a = 50$ and $h_c/h_f = 20$. The results indicate that the non-dimensional deflection values are increasing with an increase in the load parameter (Q). It is noted from the results that the deflection values are decreasing as the end support condition changes from, CFCF, SSSS, CSCS, and CCCC. In addition, the results show that the deflection values are higher for the cross-ply $(0^\circ/90^\circ/\text{Core}/90^\circ/0^\circ)$ lamination when compared to angle-ply $(45^\circ/-45^\circ/\text{Core}/-45^\circ/45^\circ)$ sandwich panel.

Finally, one more example is solved to show the variation of the deflection and the normal stress values for different geometries. The responses are obtained under uniformly distributed loading for the square simply-supported cross-ply $(0^\circ/90^\circ/\text{C}/90^\circ/0^\circ)$ sandwich shell panel using M2 properties and presented in Table 4. For the computational purpose, the responses are obtained using the various geometrical parameters i.e., $a/h = 5, 10, 15$ and 20 ; $R/a = 5, 10, 20$ and 50 . It is observed from the responses that the deflection values are decreasing with an increase in the side-to-thickness ratio (a/h) and the reverse trend follows with an increase in the curvature ratio (R/a). In addition, the in-plane normal stress values are following the same trend. It is also observed that the results are following the decreasing trend when the geometry of the structure changes from, Hyp, Cyl, Elpt, and Sph.

Now, a square three-layered $(0^\circ/\text{C}/0^\circ)$ simply-supported spherical sandwich shell panel ($a/h = 80$) under sinusoidal loading is analysed for the normal and the shear stresses through the panel thickness. The non-dimensional stresses are obtained using M3 material property for different curvature ratios ($R/a = 10, 20, 30, 40$ and 50) and presented in Fig. 10. From the figure, it can be seen that for almost all the cases the stress values are increasing while the curvature ratio increase. In general, the stresses are symmetric in nature for the symmetric laminate, however, in the present case there is some discrepancies due to the consideration of the geometrical nonlinearity.

5 Conclusions

The nonlinear static responses of the skew sandwich composite shell (cylindrical/spherical/elliptical/hyperbolic) panel is analysed in the present article. The desired responses are obtained computationally with the help of customized computer code (MATLAB environment) via geometrically nonlinear FE model and the direct iterative method. The current model includes all of the higher-order nonlinear strain terms to compute the exact structural flexure. The effectiveness

of the presently proposed and developed numerical model is checked by convergence and comparison study. Finally, few sets of numerical examples have been solved to explore the influence of the various geometrical parameters on the non-dimensional static responses of the sandwich composite structure. The computed responses (deflection and stress) indicate that the Sph panels are most robust structural panel while compared to other geometries (Cyl, Elpt, Hyp and FP). The deflection values are following an increasing trend with the increase of mechanical load parameter irrespective of geometries. However, the central deflections of the skew sandwich panel for the lamination schemes follow a variable behaviour due to multiple parameters variation i.e. either related to the geometrical shape or sizes.

References

1. Ren-huai L (1993) Nonlinear bending of simply supported rectangular sandwich plates. *Appl Math Mech* 14:217–234
2. Pilipchuk VN, Berdichevsky VL, Ibrahim RA (2010) Thermo-mechanical coupling in cylindrical bending of sandwich plates. *Compos Struct* 92:2632–2640
3. Sturzenbecher R, Hofstetter K (2011) Bending of cross-ply laminated composites: an accurate and efficient plate theory based upon models of Lekhnitskii and Ren. *Compos Struct* 93:1078–1088
4. Ferreira AJM, Carrera E, Cinefra M, Roque CMC (2013) Radial basis functions collocation for the bending and free vibration analysis of laminated plates using the Reissner-Mixed Variational Theorem. *Eur J Mech A Solids* 39:104–112
5. Ferreira AJM, Viola E, Tornabene F, Fantuzzi N, Zenkour AM (2013) Analysis of sandwich plates by generalized differential quadrature method. *Math Probl Eng*. <https://doi.org/10.1155/2013/964367>
6. Nguyen MN, Bui TQ, Truong TT, Tanaka S, Hirose S (2017) Numerical analysis of 3-D solids and composite structures by an enhanced 8-node hexahedral element. *Finite Elem Anal Des* 131:1–16
7. Topal U, Uzman U (2008) Strength optimization of laminated composite plates. *J Compos Mater* 42:1731–1746
8. Kheirikhah MM, Babaghasabha V (2016) Bending and buckling analysis of corrugated composite sandwich plates. *J Braz Soc Mech Sci Eng* 38:2571–2588
9. Reddy BS, Reddy AR, Kumar JS, Reddy KVK (2012) Bending analysis of laminated composite plates using finite element method. *Int J Eng Sci Technol* 4:177–190
10. Liang-bo D (1989) Bending and vibration of composite laminated plates. *Appl Math Mech* 10:345–352
11. Kumar A, Singha MK, Tiwari V (2017) Nonlinear bending and vibration analyses of quadrilateral composite plates. *Thin Wall Struct* 113:170–180
12. Do TV, Bui TQ, Yu TT, Pham DT, Nguyen CT (2017) Role of material combination and new results of mechanical behaviors for FG sandwich plates in thermal environment. *J Comput Sci* 21:164–181
13. Lee LJ, Fan YJ (1996) Bending and vibration analysis of composite sandwich plates. *Comput Struct* 60:103–112
14. Mehrabian M, Golmakani ME (2015) Nonlinear bending analysis of radial-stiffened annular laminated sector plates with dynamic relaxation method. *Comput Math Appl* 69:1272–1302

15. Srinivas S, Rao AK (1970) Bending, vibration and buckling of simply supported thick orthotropic rectangular plates and laminates. *Int J Solids Struct* 6:1463–1481
16. Butalia TS, Kant T, Dixit VDT (1990) Performance of heterosis element for bending of skew rhombic plates. *Comput Struct* 34:23–49
17. Cui XY, Liu GR, Li GY (2011) Bending and vibration responses of laminated composite plates using an edge-based smoothing technique. *Eng Anal Bound Elem* 35:818–826
18. Muhammad T, Singh AV (2004) A p-type solution for the bending of rectangular, circular, elliptic and skew plates. *Int J Solids Struct* 41:3977–3997
19. Heydari MM, Kolahchi R, Heydari M, Abbasi A (2014) Exact solution for transverse bending analysis of embedded laminated Mindlin plate. *Struct Eng Mech* 49:661–672
20. Cetkovic M, Vuksanovic Dj (2009) Bending, free vibrations and buckling of laminated composite and sandwich plates using a layerwise displacement model. *Compos Struct* 88:219–227
21. Thai ND, D'Ottavio M, Caron JF (2013) Bending analysis of laminated and sandwich plates using a layer-wise stress model. *Compos Struct* 96:135–142
22. Cetkovic M (2015) Thermo-mechanical bending of laminated composite and sandwich plates using layerwise displacement model. *Compos Struct* 125:388–399
23. Kolahchi R (2017) A comparative study on the bending, vibration and buckling of viscoelastic sandwich nano-plates based on different nonlocal theories using DC, HDQ and DQ methods. *Aerosp Sci Technol* 66:235–248
24. Shariyat M (2010) A generalized high-order global-local plate theory for nonlinear bending and buckling analyses of imperfect sandwich plates subjected to thermo-mechanical loads. *Compos Struct* 92:130–143
25. Sheikh AH, Chakrabarti A (2003) A new plate bending element based on higher-order shear deformation theory for the analysis of composite plates. *Finite Elem Anal Des* 39:883–903
26. Taj G, Chakrabarti A (2013) An Efficient C^0 finite element approach for bending analysis of functionally graded ceramic-metal skew shell panels. *J Solid Mech* 5:47–62
27. Chalak HD, Chakrabarti A, Sheikh AH, Iqbal MA (2014) C^0 FE model based on HOZT for the analysis of laminated soft core skew sandwich plates: bending and vibration. *Appl Math Modell* 38:1211–1223
28. Chakrabarti A, Sheikh AH (2005) Analysis of laminated sandwich plates based on interlaminar shear stress continuous plate theory. *J Eng Mech* 131:377–384
29. Mahi A, Adda Bedia EA, Tounsi A (2015) A new hyperbolic shear deformation theory for bending and free vibration analysis of isotropic, functionally graded, sandwich and laminated composite plates. *Appl Math Model* 39:2489–2508
30. Kolahchi R, Bidgoli AMM, Heydari MM (2015) Size-dependent bending analysis of FGM nano-sinusoidal plates resting on orthotropic elastic medium. *Struct Eng Mech* 55:1001–1014
31. Zhou Y, Zhu J (2016) Vibration and bending analysis of multiferoic rectangular plates using third-order shear deformation theory. *Compos Struct* 153:712–723
32. Sreehari VM, George LJ, Maiti DK (2016) Bending and buckling analysis of smart composite plates with and without internal flaw using an inverse hyperbolic shear deformation theory. *Compos Struct* 138:64–74
33. Bui TQ, Do TV, Ton LHT, Doan DH, Tanaka S, Pham DT, Nguyen-Van TA, Yu TT, Hirose S (2016) On the high temperature mechanical behaviors analysis of heated functionally graded plates using FEM and a new third-order shear deformation plate theory. *Compos Part B* 92:218–241
34. Do TV, Nguyen DK, Duc ND, Doan DH, Bui TQ (2017) Analysis of bi-directional functionally graded plates by FEM and a new third-order shear deformation plate theory. *Thin Walled Struct* 119:687–699
35. Bui TQ, Nguyen MN, Zhang C (2011) An efficient meshfree method for vibration analysis of laminated composite plates. *Comput Mech* 48:175–193
36. Bui TQ, Khosravifard A, Zhang Ch, Hematiyan MR, Golub MV (2013) Dynamic analysis of sandwich beams with functionally graded core using a truly meshfree radial point interpolation method. *Eng Struct* 47:90–104
37. Yin S, Yu TT, Bui TQ, Nguyen MN (2015) Geometrically nonlinear analysis of functionally graded plates using isogeometric analysis. *Eng Comput* 32:519–558
38. Yu TT, Yin S, Bui TQ, Hirose S (2015) A simple FSDT-based isogeometric analysis for geometrically nonlinear analysis of functionally graded plates. *Finite Elem Anal Des* 96:1–10
39. Walker M, Hamilton R (2007) A technique for optimally designing fibre-reinforced laminated structures for minimum weight with manufacturing uncertainties accounted for. *Eng Comput* 21:282–288
40. Upadhyay AK, Shukla KK (2013) Non-linear static and dynamic analysis of skew sandwich plates. *Compos Struct* 105:141–148
41. Lal A, Singh BN, Anand S (2011) Nonlinear bending response of laminated composite spherical shell panel with system randomness subjected to hygro-thermo-mechanical loading. *Int J Mech Sci* 53:855–866
42. Nguyen TN, Thai CH, Nguyen-Xuan H (2016) On the general framework of high order shear deformation theories for laminated composite plate structures: a novel unified approach. *Int J Mech Sci* 110:242–255
43. Nguyena TN, Ngo TD, Nguyen-Xuan H (2017) A novel three-variable shear deformation plate formulation: theory and Isogeometric implementation. *Comput Methods Appl Mech Eng* 326:376–401
44. Thai CH, Nguyen TN, Rabczuk T, Nguyen-Xuan H (2016) An improved moving Kriging meshfree method for plate analysis using a refined plate theory. *Comput Struct* 176:34–49
45. Thai CH, Ferreira AJM, Nguyen-Xuan H (2017) Naturally stabilized nodal integration meshfree formulations for analysis of laminated composite and sandwich plates. *Compos Struct* 178:260–276
46. Nguyen NV, Nguyen HX, Phan DH, Nguyen-Xuan H (2017) A polygonal finite element method for laminated composite plates. *Int J Mech Sci* 133:863–882
47. Dash P, Singh BN (2010) Geometrically nonlinear bending analysis of laminated composite plate. *Commun Nonlinear Sci Numer Simul* 15:3170–3181
48. Singh VK, Mahapatra TR, Panda SK (2016) Nonlinear flexural analysis of single/doubly curved smart composite shell panels integrated with PFRC actuator. *Eur J Mech A Solids A Solids* 60:300–314
49. Mahapatra TR, Kar VS, Panda SK (2016) Large amplitude bending behaviour of laminated composite curved panels. *Eng Comput* 33:116–138
50. Jones RM (1999) *Mechanics of composite materials*. Taylor & Francis, Philadelphia
51. Cook RD, Malkus DS, Plesha ME, Witt RJ (2003) *Concepts and applications of finite element analysis*. Wiley, Singapore
52. Reddy JN, (2003) *Mechanics of laminated composite: plates and shells—theory and analysis*. CRC Press, Boca Raton
53. Pagano NJ (1970) Exact solutions for rectangular bidirectional composites and sandwich plates. *J Comput Math* 4:20–34
54. Kant T, Gupta AB, Pendhari SS, Desai YM (2008) Elasticity solution for cross-ply composite and sandwich laminates. *Compos Struct* 83:13–24
55. Pagano NJ (1970) Exact solution of rectangular bidirectional composites and sandwich plates. *J Compos Mater* 4:20–34

56. Pandya BN, Kant T (1988) Higher-order shear deformation theories for flexure of sandwich plates-finite element evaluations. *Int J Solids Struct* 24:1267–1286
57. Wu CP, Kuo HC (1993) An interlaminar stress mixed finite element method for the analysis of thick laminated composite plates. *Compos Struct* 24:29–42
58. Ramtekkar GS, Desai YM, Shah AH, (2002) Mixed finite element model for thick composite laminated plates. *Mech Adv Mater Struct* 9:133–156

Publisher's Note Springer Nature remains neutral with regard to jurisdictional claims in published maps and institutional affiliations.